

修士論文

乳房超音波画像における腫瘍病変の
病理組織型の自動分類法

**Computerized Classification Method for Determining
Histological Classifications of Breast Masses on
Ultrasonographic Images**

平成 22 年度修了

三重大学大学院 工学研究科

博士前期課程 電気電子工学専攻

檜作 彰良

Contents

1. Introduction	1
1.1 Breast cancer	1
1.2 Ultrasonography and Mammography.....	2
1.3 Purpose of this study	3
2. Materials.....	5
3. Methods	6
3.1 Segmentation of mass.....	7
3.1.1 Snakes technique	7
3.1.2 Region-growing technique	10
3.2 Segmentation of mass.....	11
3.3 Extraction of nine objective features	16
3.3.1 Depth-width ratio	16
3.3.2 Degree of circularity.....	17
3.3.3 Degree of shape irregularity	18
3.3.4 Degree of indistinctness in margin.....	19
3.3.5 Degree of irregularity in margin.....	20
3.3.6 Heterogeneousness in internal echoes.....	21
3.3.7 Intensity of echo-level in internal echoes.....	22
3.3.8 Degree of echo-level in posterior echoes	23
3.3.9 Degree of lateral shadows	24
3.4 Extraction of nine objective features	25
4. Results.....	25
5. Discussion	28

6. Conclusion	36
Acknowledgment	36
Reference	37
Research Accomplishment	39

Figure caption

Figure1	Number of women who died of breast cancer in Japan	1
Figure2	Example of four masses with different types of histological classifications	5
Figure3	Schematic diagram of the proposed methods	6
Figure4	Example of the parametric expression of closed curve	7
Figure5	Example of the region-growing technique	10
Figure6	Example of the mass region segmented by the proposed method. (a) Original image, (b) smoothed image, (c) mass region extracted roughly by the Snakes technique, and (d) the boundary line (white line) for the mass region segmented by the region growing technique.....	12
Figure7	Example of the mass region segmented by the proposed method. (a) Original image, (b) smoothed image, (c) mass region extracted roughly by the Snakes technique, and (d) the boundary line (white line) for the mass region segmented by the region growing technique.....	13
Figure8	Example of the mass region segmented by the proposed method. (a) Original image, (b) smoothed image, (c) mass region extracted roughly by the Snakes technique, and (d) the boundary line (white line) for the mass region segmented by the region growing technique.....	14
Figure9	Example of the mass region segmented by the proposed method. (a) Original image, (b) smoothed image, (c) mass region extracted roughly by the Snakes technique, and	

(d) the boundary line (white line) for the mass region segmented by the region growing technique.....	15
Figure10 Example of depth and width	16
Figure11 Example of the outline for the segmented mass	17
Figure12 Example of the definition of the shape factors for the segmented mass. (a) Eight shape factors are the minimum lengths of the distance, and (b) eight shape factors are the maximum lengths of the distance between the center-of-mass pixel and the edge of mass in eight regions separated by 45 degree	18
Figure13 Example of inside band and outside band.....	19
Figure14 Example of the outside in the mass and perimeter of the circle. (a) Outside in the segmented mass, (b) perimeter of the circle (a circle with the same area as the mass region)	20
Figure15 Example of internal echoes region.....	21
Figure16 Example of internal echoes region.....	22
Figure17 Example of anterior region and posterior region	23
Figure18 Example of anterior region and lateral regions.....	24
Figure19 Relationship between depth-width ratio and degree of indistinctness in margin.....	30
Figure20 Relationship between degree of circularity and degree of shape irregularity	31
Figure21 Relationship between heterogeneousness in internal echoes and intensity of echo-level in internal echoes.....	32
Figure22 Relationship between degree of echo-level in posterior echoes and degree of lateral shadows	33
Figure23 Relationship between degree of indistinctness in margin and degree of irregularity in margin	34

Table caption

Table I Compare of mammography to ultrasonography 2

Table II Automated classification results for masses among the four histological
 classifications 27

Table III Tests for univariate equality of group means 35

Introduction

1.1 Breast cancer

Breast cancer is one of major problems for woman health in developed countries. In the United States, one in eight women has breast cancer during their lives [1]. Therefore, it is estimated that about 40,000 people will die of breast cancer in a year. In Japan, MHLW (Ministry of Health, Labor and Welfare) reported that one in about sixteen women has breast cancer during their lives. The number of women who died of breast cancer was 11,918 in 2009 [2]. Breast cancer has had the highest disease rate in all the cancers for Japanese women. Figure 1 shows the change in the numbers of women who died of breast cancer in Japan. It is expected that the number of people who die of breast cancer will increase for some time because the disease rate of breast cancer continues to increase. To overcome this issue, it is necessary to treat breast cancer at early stage before a subjective symptom such as lump appears.

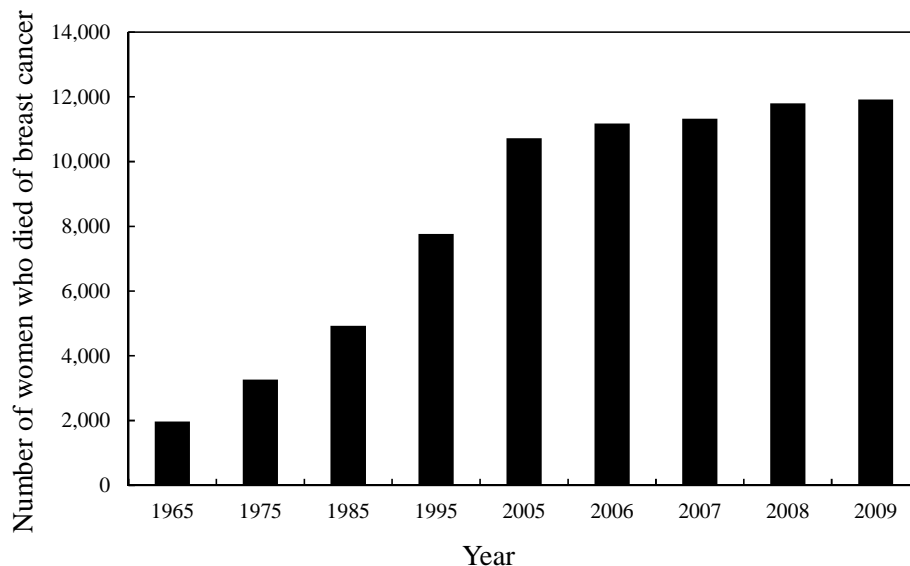


Figure 1 Number of women who died of breast cancer in Japan.

1.2 Ultrasonography and mammography

Mammography which is x-ray for breast is considered the most effective method for detection of early breast cancer. Breast cancer examination in Japan must be implemented based on mammography. However, it is often difficult to detect lesions in mammograms for young women (30-40 years old) because most of young Japanese women have dense breast.

Especially, mass which is one of important indications related to breast cancer is hidden in the grown mammary gland structure on the dense breast. On the other hand, it is known that it is easier to detect masses on ultrasonographic images than mammograms because an ultrasonography (US) which is an examination with sound waves is influenced hardly by the grown mammary gland structure. Therefore, to use both mammography and the US is recommended in breast cancer examination. Here, clustered microcalcifications which is one of important indications is required to be detected and diagnosed mainly at mammography, whereas mass is required to be detected and diagnosed mainly at ultrasonography. Table I shows compare of mammography to ultrasonography.

Table I. Compare of mammography to ultrasonography.

	Merit	Demerit
Mammography	It is easy to detect clustered microcalcifications	It is very difficult to distinguish breast cancer (microcalcifications and mass) and mammary gland for young women
Ultrasonography	It is easy to detect mass	It is difficult to detect clustered microcalcifications

1.3 Purpose of this study

Clinicians detect a mass on ultrasonographic image and then determine whether the mass is malignant or benign. Here, malignant mass is mistakenly diagnosed as benign lesion on rare occasions, and is overlooked. On the other hand, the positive predictive value of ultrasonography, i.e., the ratio of the number of breast cancers found to the number of biopsies, is rather low. Unnecessary biopsies cause patients both physical and costly problem. In order to reduce the number of unnecessary biopsies, experienced clinicians evaluate not only the likelihood of malignancy but also the likelihood of a histological classification. They then decide on patient managements based on the likelihood of histological classifications.

To improve the positive predictive value, in the previous studies, many investigators have attempted to develop a discriminant method for distinguishing between benign and malignant breast masses on ultrasonographic images. Chen *et al.* [3] developed a computer-aided diagnosis (CADx) for differentiating malignant masses from benign masses by use of an artificial neural network (ANN) with acoustic features. Joo *et al.* [4] also employed an ANN with morphologic features. Nicholas *et al.* [5] extracted four objective features of masses on ultrasonographic images. These four objective features were lesion shape, margin sharpness, posterior acoustic shadowing, and lesion texture. They estimated the likelihood of malignancy by using Bayesian neural network (BNN) with these features. The results of these discriminant methods indicated a high performance for distinguishing between benign and malignant breast masses.

Making clinical decisions for biopsy or follow-up on breast masses by taking into account possible histological classifications on ultrasonographic images may reduce the number of unnecessary biopsies [6, 7]. For example, patients with breast masses associated with invasive carcinomas that may metastasize to other organs must undergo biopsy immediately. Patients

with noninvasive carcinoma type that grows rapidly must undergo biopsy or follow-up at a very short interval of a few months [7]. Patients with cysts and fibroadenomas which are benign breast lesions can have follow-up at a relatively long interval of six months [7]. Therefore, the computerized analysis for evaluating the likelihood of histological classifications and also the likelihood of malignancy for breast masses would be helpful to clinicians for their decisions on patient management.

The purpose of this study is to develop a computerized classification method for histological classifications of breast masses on ultrasonographic images in order to assist clinicians' interpretation as a "second opinion." In this study, we first extract nine objective features by taking into account subjective terms that clinicians commonly use for describing breast masses. These objective features are: (1) Depth-width ratio, (2) the degree of circularity, (3) the degree of shape irregularity, (4) the degree of indistinctness in margin, (5) the degree of irregularity in margin, (6) Heterogeneous in internal echoes, (7) Intensity of echo-level in internal echoes, (8) the degree of echo-level in posterior echoes, and (9) the degree of lateral shadows. We propose a classification method based on the difference in nine objective features among four histological classifications. The performance of this proposed method is evaluated by 83 breast ultrasonographic images.

2. Materials

Our database consisted of 83 breast ultrasonographic images obtained from 83 patients at Mie University Hospital, Tsu, Japan. It included 40 malignant masses (25 invasive carcinomas and 15 noninvasive carcinomas) and 43 benign masses (17 cysts and 26 fibroadenomas). The histological classifications of these masses were proved by pathologic diagnosis. These ultrasonographic images were size of 716 by 537 pixels, 8 bit gray scale. Figure 2 shows an example of four masses with different types of histological classifications.

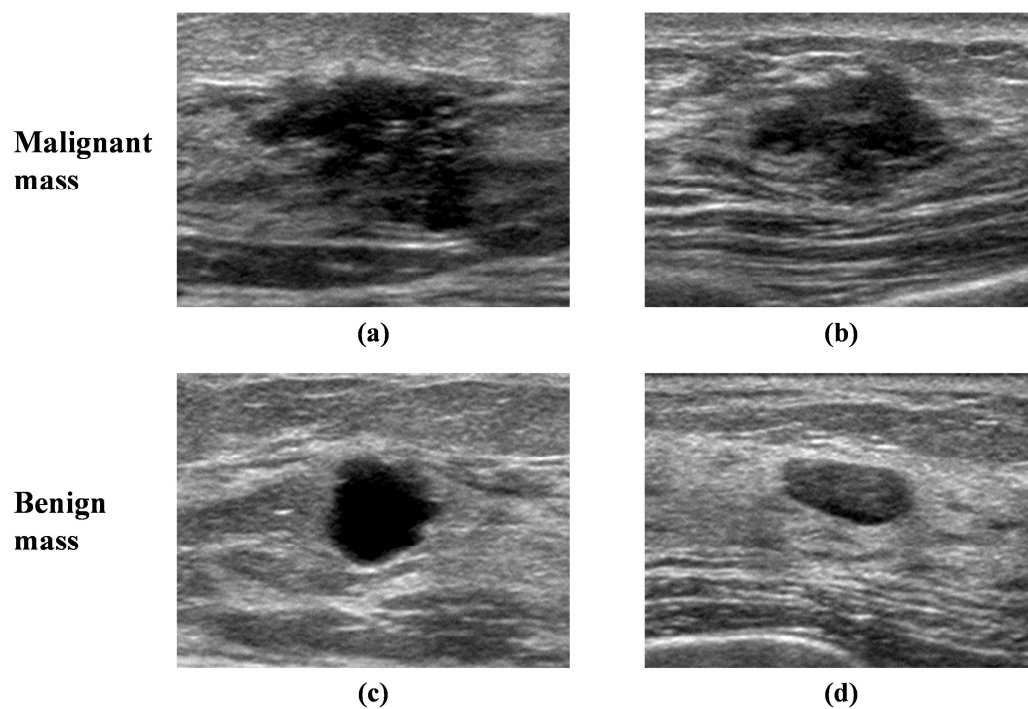


Figure 2 Example of four masses with different types of histological classifications, (a) Invasive carcinoma, (b) noninvasive carcinoma, (c) cyst, (d) fibroadenoma.

3. Methods

Figure 3 shows a schematic diagram of the proposed method of histological classifications for breast masses on ultrasonographic images.

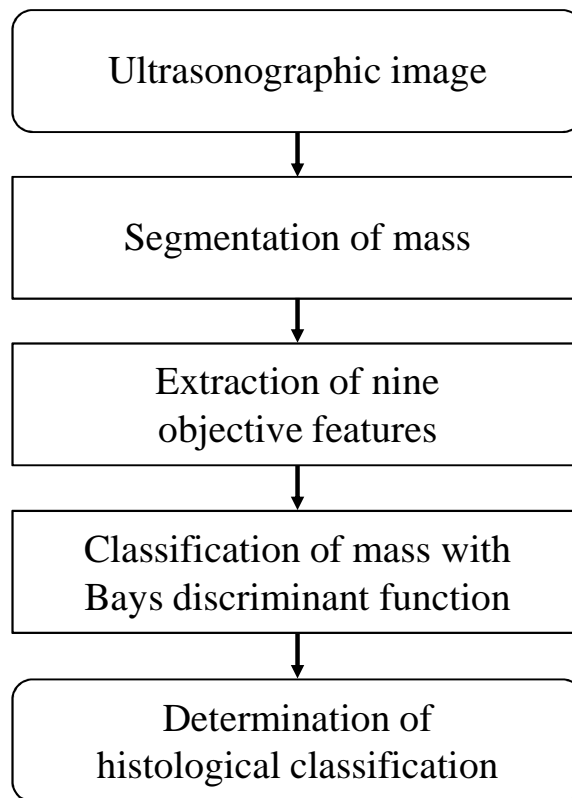


Figure 3 Schematic diagram of the proposed method.

3.1 Segmentation of mass

In order to segment mass region accurately, the proposed method uses both a Snakes technique and a region growing technique. To support readability of this paper, we briefly describe them here.

3.1.1 Snakes technique

A Snakes technique [8] is one of the region extraction techniques. A closed curve of energy (E) for the Snakes technique is defined by following equation. The minimum of the closed curve of energy is supposed to be a curve which approximates a boundary of the object of interest. The closed curve of energy for the snakes is given by

$$E = \int_0^1 E_{\text{int}}(v(s))ds + \int_0^1 E_{\text{image}}(v(s))ds . \quad (1)$$

Here, the Snakes technique which is defined parametrically by $v(s) = (x(s), y(s))$, $s \in [0, 1]$ is a curve (Figure 4).

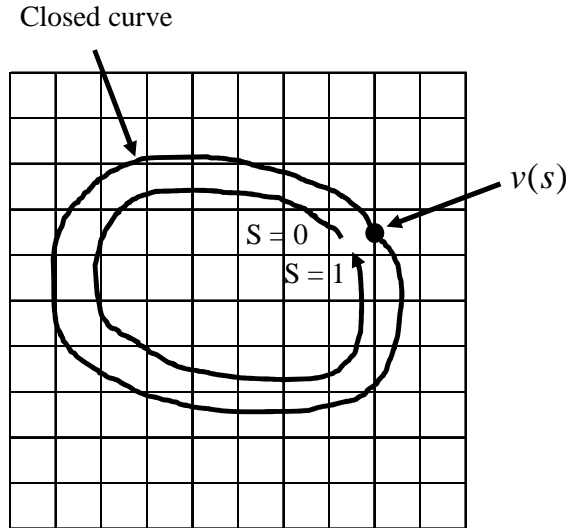


Figure 4 Example of the parametric expression of closed curve.

E_{int} is the internal energy that expresses the smoothness or the continuity of contours. E_{int} is given by

$$E_{\text{int}} = \frac{I}{2} (\alpha |v_s(s)|^2 + \beta |v_{ss}(s)|^2). \quad (2)$$

Here, $v_s \left(= \left| \frac{dv}{ds} \right|^2 \right)$ and $v_{ss} \left(= \left| \frac{d^2v}{ds^2} \right|^2 \right)$ are the first difference and the second difference,

respectively. v_s indicates the continuity of closed curve. v_{ss} also indicates the smoothness of closed curve. α and β are weight coefficients. On the other hand, E_{image} is the image energy based on the edge of the closed curve. E_{image} becomes smaller on the edge because it produces shrink force into closed curve. E_{image} is given by

$$E_{\text{image}} = -|\nabla I(v(s))|. \quad (3)$$

Here, $\nabla I(v(s))$ indicates the gradient of pixel values at $v(s)$. However, it is known that this method would not accurately segment a crossed curve with sharp flexion. Xu *et.al* [9, 10] proposed active contour model which modify contour based on gradient vector flow of image. This model defines an edge map $f(x, y)$ derived from the image $I(x, y)$. The edge map $f(x, y)$ is given by

$$f(x, y) = -E_{\text{image}}^i(x, y). \quad (4)$$

The properties of edge map ∇f have: (1) vectors pointing toward the edges, (2) large magnitudes in only surrounding area of the edges, and (3) ∇f is nearly zero in homogeneous regions where $I(x, y)$ is nearly constant. The gradient vector flow field is defined by $v(x, y) = [u(x, y), v(x, y)]$ that minimizes the energy function

$$\mathcal{E} = \iint \mu(u_x^2 + u_y^2 + v_x^2 + v_y^2) + |\nabla f|^2 |v - \nabla f|^2 dx dy. \quad (5)$$

The vector field can be found by solving following Euler equations.

$$\mu \nabla^2 u - (u - f_x)(f_x^2 + f_y^2) = 0 \quad (6)$$

$$\mu \nabla^2 v - (v - f_y)(f_x^2 + f_y^2) = 0 \quad (7)$$

These equations satisfy following equations (8) and (9). The equations of (8) and (9) indicate x vector and y vector for brightness gradient vector field function. These equations are given by

$$u_t(x, y, t) = \mu \nabla^2 u(x, y, t) - [u(x, y, t) - f_x(x, y)] \cdot [f_x(x, y)^2 + f_y(x, y)^2], \quad (8)$$

$$v_t(x, y, t) = \mu \nabla^2 v(x, y, t) - [v(x, y, t) - f_y(x, y)] \cdot [f_x(x, y)^2 + f_y(x, y)^2]. \quad (9)$$

Here, u_t and v_t indicate the directions of x and y . t is repeat count, whereas μ is variable of GVF field [11].

3.1.2 Region-growing technique

A region-growing technique [12] is one of the region extraction techniques. It is a procedure that groups pixels or sub regions into larger regions based on predefined criteria. On the target region, one or more pixels are first set as the starting point for the region-growing technique. These pixels are called “seeds”. The neighboring pixels of these seeds are connected to the seeds (region) when they have characteristic close to the seeds. In this paper, the criterion for characteristic is based on the pixel values. The connected pixels are defined as new seeds. This procedure is repeated until every seed have been used once. The pixels connecting to the seeds are finally extracted as the target region (Figure 5).

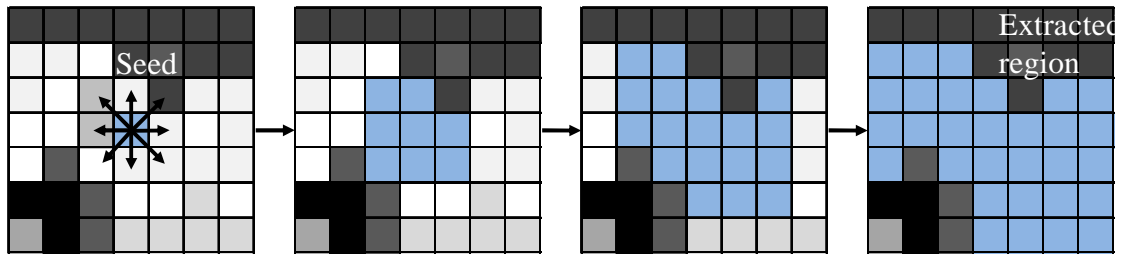


Figure 5 Example of the region-growing technique.

3.2 Segmentation of mass

In the proposed method, ultrasonographic image (Figure 6-9 (a)) is first smoothed by use of a median filter [12] (Figure 6-9 (b)) because there are discontinuous values caused by speckle noises. The size of the median filter is 5 pixels x 5 pixels. The mass region is then segmented by two steps. First, the Snakes technique is employed to extract roughly the mass region. Here, initial border line for the Snakes technique is set manually within the mass region by an experienced clinician. This initial border line is given by a rectangle (Figure 6-9 (c)). The region wrapped by the border line is defined as the extracted mass region when the energy function was minimized. The parameters of the Snakes technique are given empirically. Figure 6-9 (d) shows the mass region extracted roughly by the Snakes technique. However, it is difficult for the Snakes technique to segment the irregularity on the edge of the mass. Therefore, a region-growing technique is applied around the extracted mass region to segment the detailed edge of the mass region. The criteria for the region-growing is given by the average \pm the standard deviation of pixel values in mass region extracted by the Snakes technique. Figure 6-9 (e) shows the boundary line (white line) for the mass region segmented by the region-growing technique.

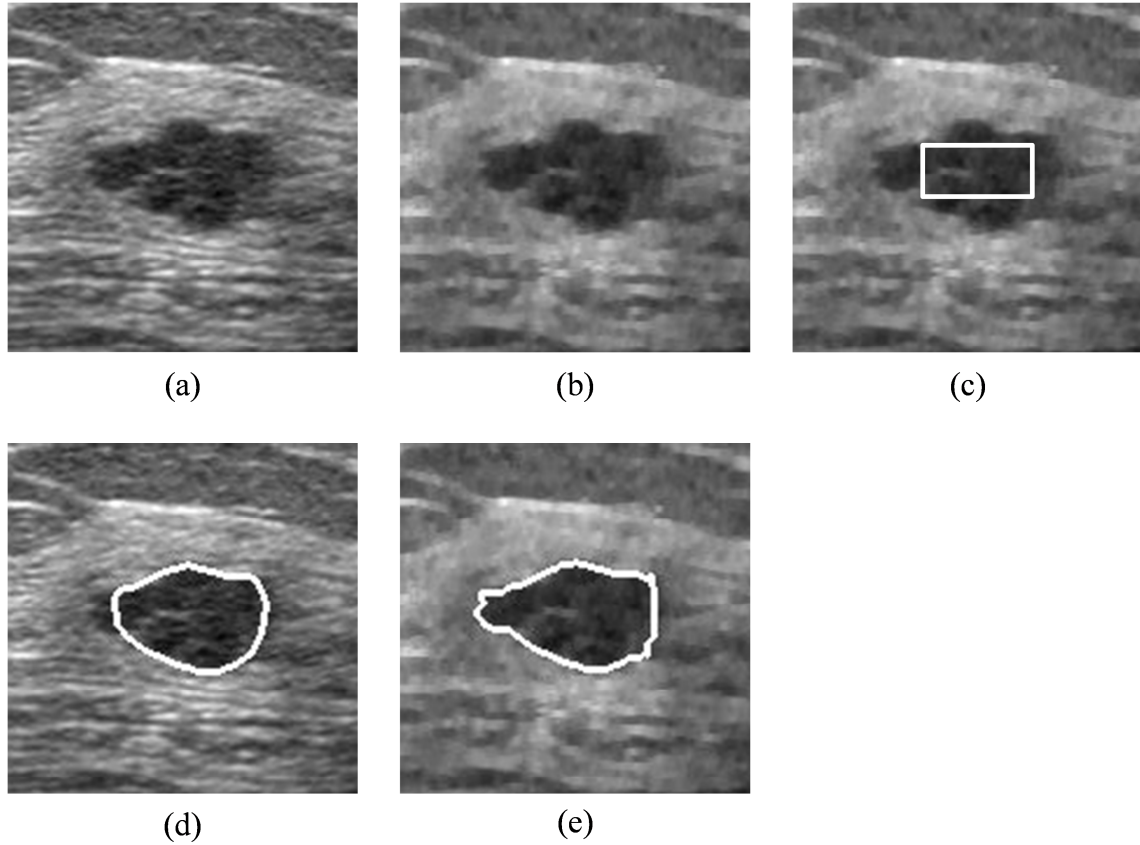


Figure 6 Example of a mass region segmented by the proposed method.
 (a) original image (b) smoothed image (c) initial border line for the Snakes technique,
 (d) mass region extracted roughly by the Snakes technique, and
 (e) the boundary line (white line) for the mass region segmented
 by the region-growing technique.

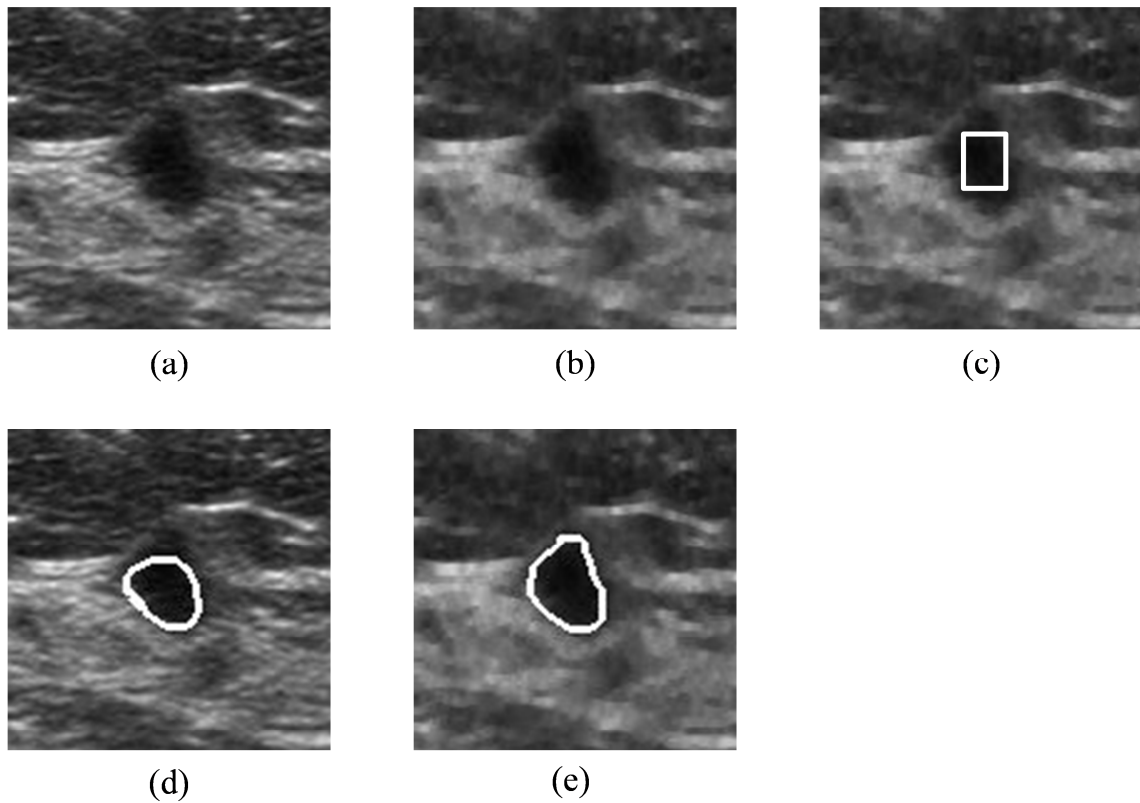


Figure 7 Example of a mass region segmented by the proposed method.
 (a) original image (b) smoothed image (c) initial border line for the Snakes technique,
 (d) mass region extracted roughly by the Snakes technique, and
 (e) the boundary line (white line) for the mass region segmented by
 the region-growing technique.

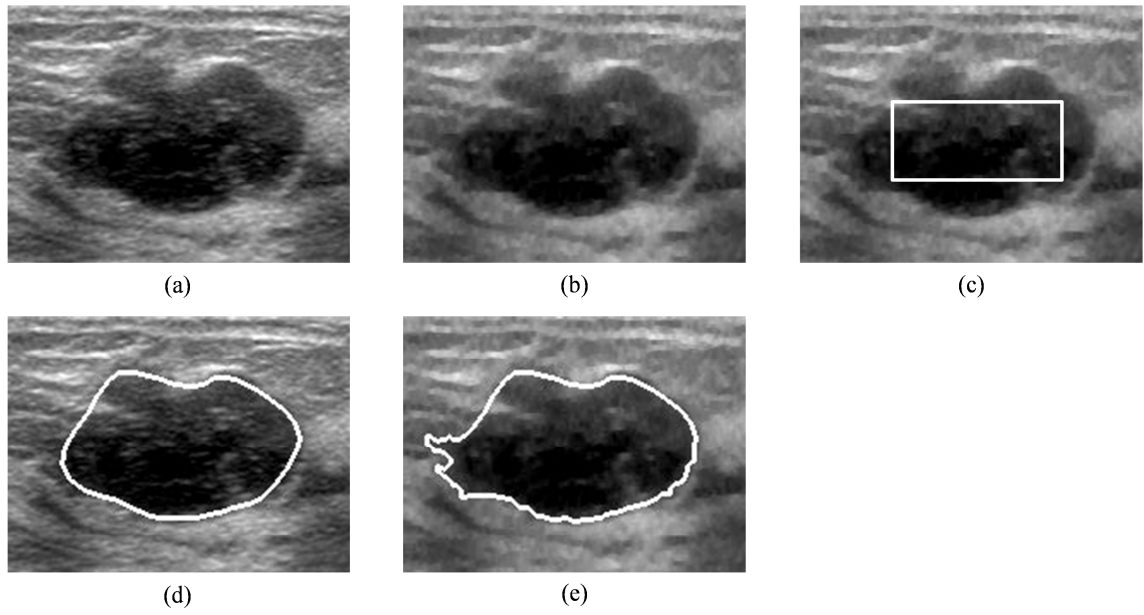


Figure 8 Example of a mass region segmented by the proposed method.
 (a) original image (b) smoothed image (c) initial border line for the Snakes technique,
 (d) mass region extracted roughly by the Snakes technique, and
 (e) the boundary line (white line) for the mass region segmented by
 the region-growing technique.

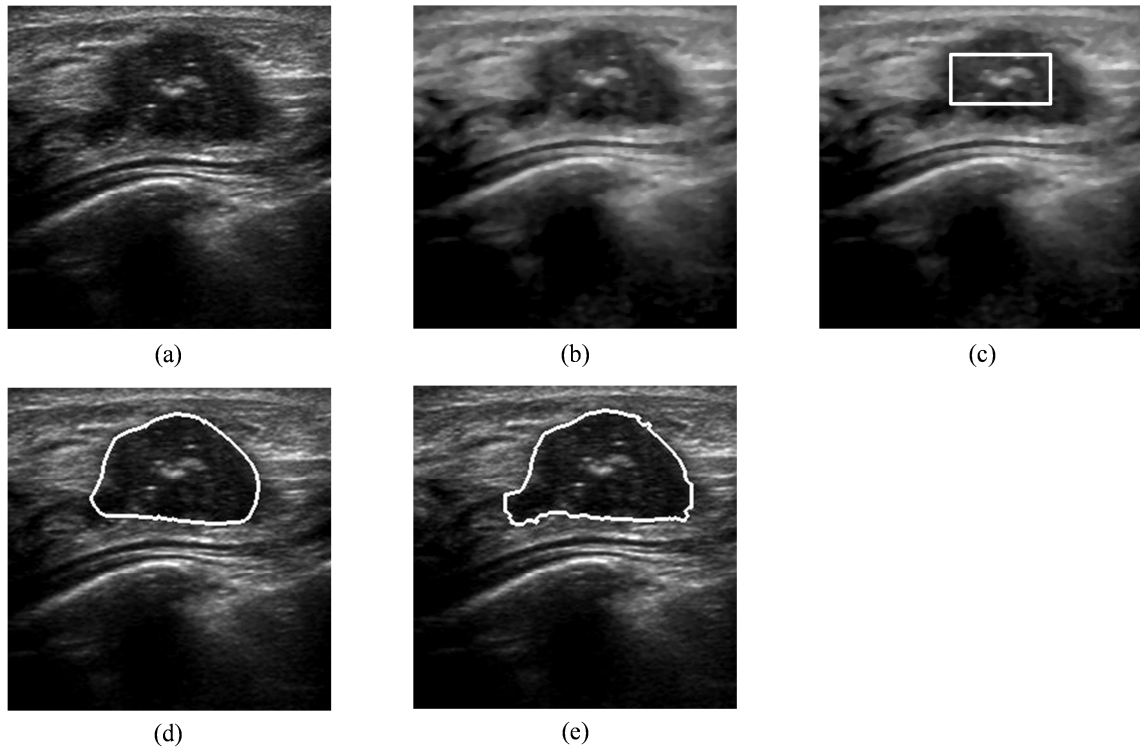


Figure 9 Example of a mass region segmented by the proposed method.
 (a) original image (b) smoothed image (c) initial border line for the Snakes technique,
 (d) mass region extracted roughly by the Snakes technique, and
 (e) the boundary line (white line) for the mass region segmented by
 the region-growing technique.

3.3 Extraction of nine objective features

Nine objective features on mass region are determined by taking into account image features that experienced clinicians commonly use for describing breast masses on ultrasonographic images.

3.3.1 Depth-width ratio

Depth-width ratio is determined by the ratio of the maximum chord at vertical direction and the maximum chord at horizontal direction in the mass region. Figure 10 shows an example of the depth and width. It is known that benign mass tends to have high depth-width ratio.

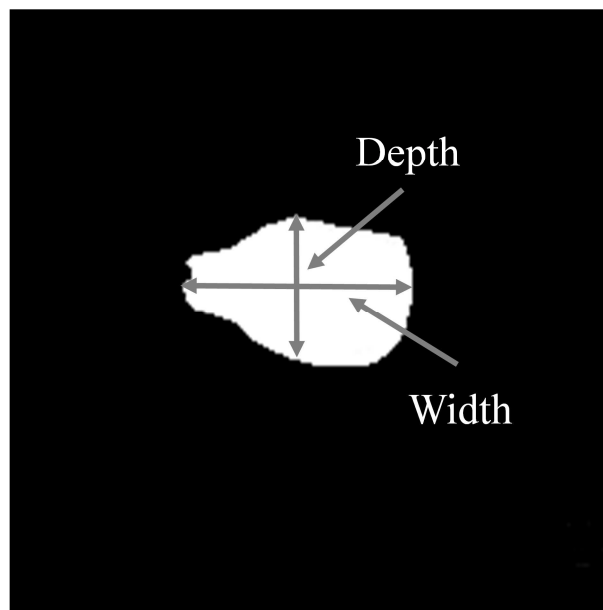


Figure 10 Example of depth and width.

3.3.2 Degree of circularity

The degree of circularity is given by

$$\text{degree of circularity} = \frac{4 \times \pi \times \text{Area}}{(\text{Length of the outline})^2}. \quad (10)$$

Here, area is the number of pixels within the mass region, whereas length of the outline is the number of pixels on the margin of the mass region. Figure 11 shows an example of the outline for the segmented mass. Benign mass tends to have high degree of circularity.

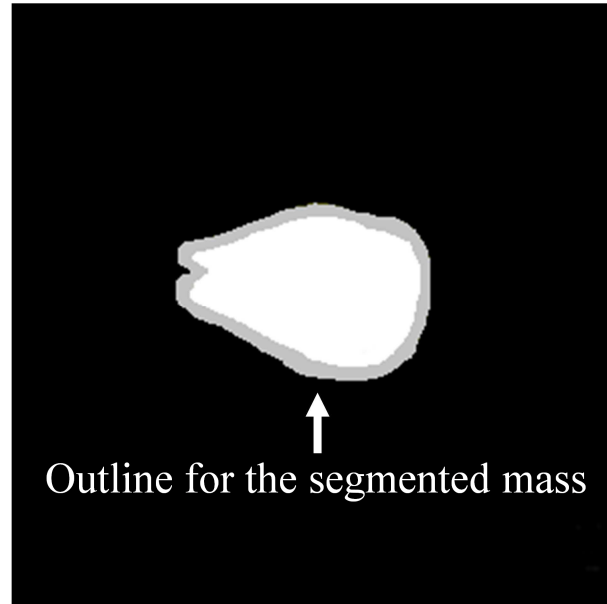


Figure 11 Example of the outline for the segmented mass.

3.3.3 Degree of shape irregularity

In order to determine the degree of shape irregularity, we first define 16 shape factors for the mass. The 16 shape factors consisted of 8 minimum distances (Figure 12(a)) and 8 maximum distances (Figure 12(b)) between the center of the breast mass and the edges of the breast mass. The minimum distance and the maximum distance are obtained in each of 8 regions located at intervals of 45 degrees. The degree of shape irregularity is then determined by the standard deviation of these 16 shape factors. For breast mass with round shape, all 16 shape factors would have similar values; thus the standard deviation would be small. For breast mass with irregular shape, some of the 16 shape factors have large values, whereas others have small values; therefore, the standard deviation would be large. Malignant mass tends to have high degree of shape irregularity.

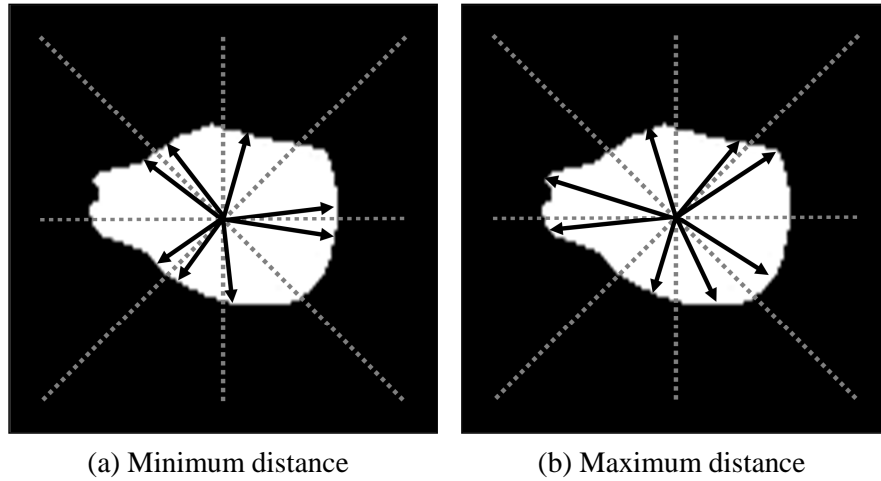


Figure 12 Example of the definition of the shape factors for the segmented mass, (a) Eight shape factors are the minimum lengths of the distance, and (b) eight shape factors are the maximum lengths of the distance between the center-of-mass pixel and the edge of mass in eight regions separated by 45 degree.

3.3.4 Degree of indistinctness in margin

A degree of indistinctness in margin is determined by the ratio of the mean pixel value in the outside band and the mean pixel value in the inside band. The degree of indistinctness in margin is given by

$$\text{The degree of indistinctness in margin} = \frac{\text{Mean pixel value in inside band}}{\text{Mean pixel value in outside band}}. \quad (11)$$

Here, outside band is outside region with 5 pixels width around the margin of the mass region, whereas inside band is inside region with 5 pixels width around the margin of the mass region.

Margin for malignant cases tends to be more indistinct than that for benign cases. Figure 13 shows an example of the inside band and the outside band.

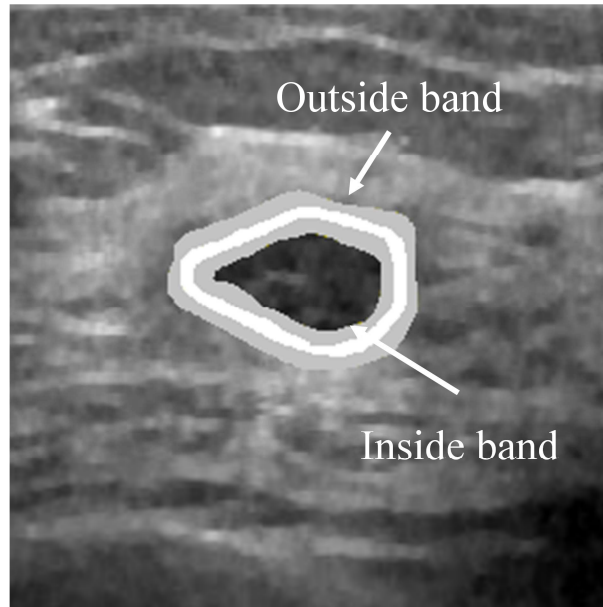


Figure 13 Example of inside band and outside band.

3.3.5 Degree of irregularity in margin

A degree of irregularity in margin is determined by the ratio of the length of the outline in the segmented mass and the perimeter of a circle with the same area as the segmented mass region. The degree of irregularity in margin is given by

$$\text{The degree of irregularity in margin} = \frac{\text{Length of the outline}}{\text{Perimeter of the circle}}. \quad (12)$$

When the degree of irregularity in margin is high, the mass indicates a high likelihood of malignancy. Figure 14 shows an example of the outside of the segmented mass and the perimeter of the circle.

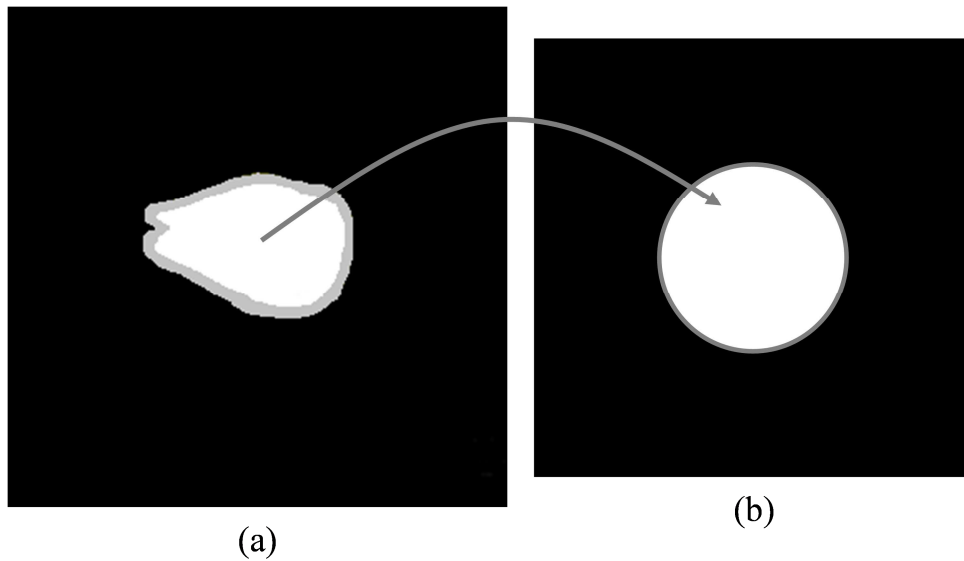


Figure 14 Example of the outside in the segmented mass and perimeter of the circle,
(a) Outside in the segmented mass,
(b) perimeter of the circle (a circle with the segmented same area as the mass region).

3.3.6 Heterogeneous internal echoes

The heterogeneous internal echoes in the segmented mass region is determined by the standard deviation of the pixel values in the segmented mass region. When the heterogeneous internal echoes is high, there is a possibility that the mass is malignant. Figure 15 shows an example of the internal echoes region.

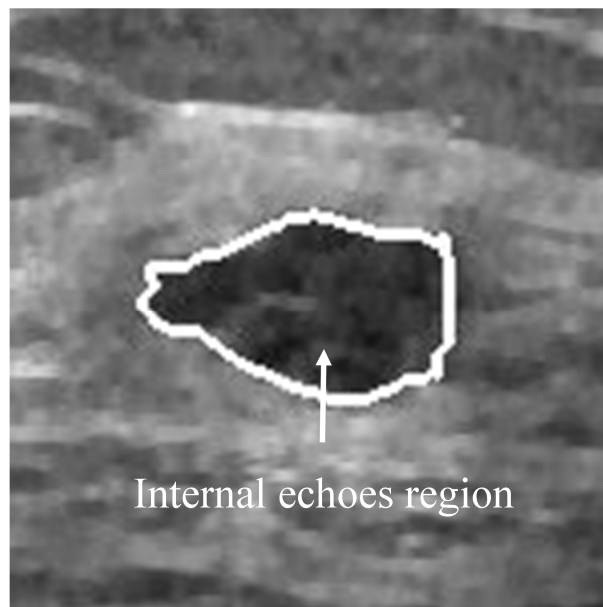


Figure 15 Example of internal echoes region.

3.3.7 Intensity of echo-level in internal echoes

An intensity of echo-level in internal echoes is determined by the average of the pixel values within the segmented mass region. When the value of average for intensity of echo-level in internal echoes is low, there is a possibility that the mass is benign. Figure 16 shows an example of the internal echoes region.

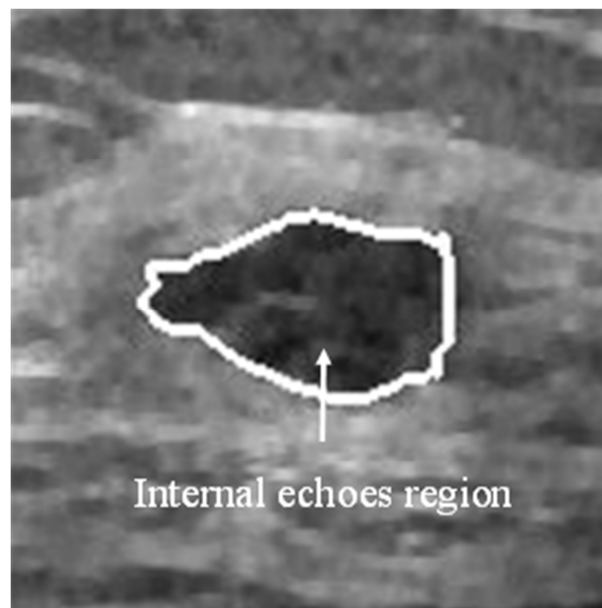


Figure 16 Example of internal echoes region.

3.3.8 Degree of echo-level in posterior echoes

A degree of echo-level in posterior echoes is determined by subtracting the mean pixel value in posterior region from the mean pixel value in anterior region. The anterior region is located anterior to the segmented mass region. The size of the anterior region is (the maximum chord at the vertical direction) x (the maximum chord at the horizontal direction). On the other hand, the posterior region is located posterior to the segmented mass region. The size of the posterior region is (the maximum chord at the vertical direction) x (the maximum chord at the horizontal direction). Benign masses tend to have high degree of echo-level in posterior echoes, whereas malignant masses have high or low degree of echo-level in posterior echoes [13, 14]. Figure 17 shows an example of the anterior region and the posterior region.

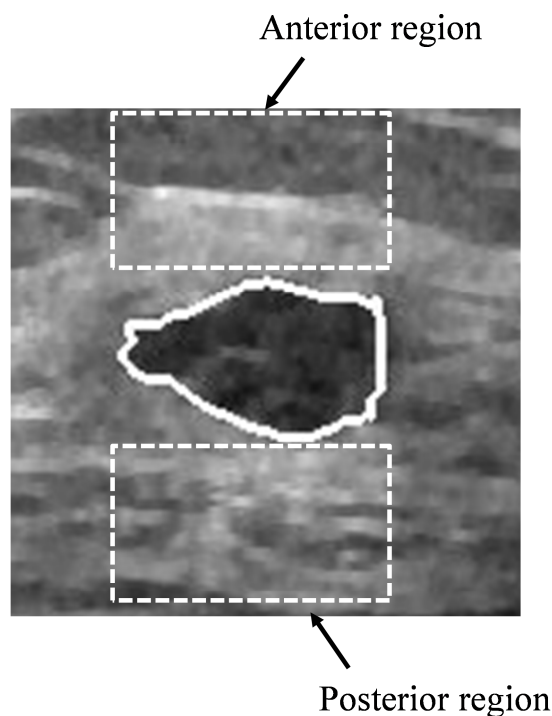


Figure 17 Example of anterior region and posterior region.

3.3.9 Degree of lateral shadows

A degree of lateral shadows is determined by subtracting the mean value in lateral regions from the mean pixel value in anterior region. The anterior region is located anterior to the segmented mass region. The size of the anterior region is 15-pixels x (the maximum chord at the horizontal direction in the segmented mass). Two lateral regions are located; one is located at the left side, whereas another is located at right side of the segmented mass. The size of lateral regions are (the maximum chord at the vertical direction in the segmented mass) x 15-pixels. The lateral shadows appear when the margin of mass is smooth. Thus, there is a possibility that the mass with the lateral shadows is benign. Figure 18 shows an example of the anterior region and the lateral regions.

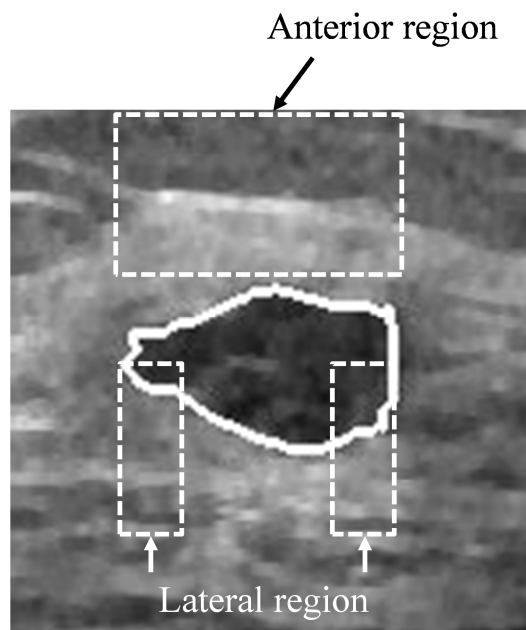


Figure 18 Example of anterior region and lateral regions.

3.4 Classification of mass with Bays discriminant function

The classifier based on Bays discriminant function [15] is employed for distinguishing between four different types of histological classifications. The Bays discriminant function is given by

$$g^l(x) = (x - \mu_l)^t \Sigma_l^{-1} (x - \mu_l) + \ln |\Sigma_l| . \quad (13)$$

μ_l : A feature vector of a mass

μ_l : Mean vector of mass in category l

Σ_l : Covariance matrix of mass in category l

For the input of the Bays discriminant function, we use nine objective features obtained from masses on ultrasonographic images. These features are normalized by use of the objective features obtained from our database. The output of the Bays discriminant function provided four values indicating the likelihood of each histological classification. The leave-one-out testing method [16, 17] is used for training and testing of the linear discriminant function. In this method, the training is carried out for all except one case in our database; the case not used for training is used for testing with the trained the linear discriminant function. This procedure is repeated until every case in our database had been used once.

4. Results

Table I shows the results of the distinction of the four histological classifications by use of the classifier based on a Bays discriminant function. The classification accuracies of this proposed method were 80.0 % (20/25) for invasive carcinomas, 73.3 % (11/15) for noninvasive carcinomas, 82.4% (14/17) for cysts, and 84.6 (22/26) % fibroadenomas, respectively. The sensitivity [18] and the specificity [18] based on the classification results of histological classification were 85.0 % (34/40) and 93.0 % (40/43), respectively. The sensitivity and specificity were defined by

$$Sensitivity = \frac{TP}{TP + FN} . \quad (13)$$

$$Specificity = \frac{TN}{TN + FP} . \quad (14)$$

True positive (TP) : malignant mass correctly identified as malignant mass.

False positive (FP) : benign mass incorrectly identified as malignant mass.

True negative (TN) : benign mass correctly identified as benign mass.

False negative (FN) : malignant mass incorrectly identified as benign mass.

The positive predictive values [18] were also 87.0 % (20/23) for invasive carcinomas, 78.6% (11/14) for noinvasive carcinomas. The negative predictive values [18] were 93.3% (14/15) for cysts, and 71.0% (22/31) for fibroadenomas. The positive predictive value and the negative predictive value were defined by

$$Positive\ predictive\ value = \frac{TP}{TP + FP} . \quad (15)$$

$$Negative\ predictive\ value = \frac{TN}{TN + FN} . \quad (16)$$

True positive (TP) : malignant mass correctly identified as malignant mass.

False positive (FP) : benign mass incorrectly identified as malignant mass.

True negative (TN) : benign mass correctly identified as benign mass.

False negative (FN) : malignant mass incorrectly identified as benign mass.

Table II Automated classification results for masses among the four histological classifications.

	Classification Accuracy			
	Invasive carcinoma	Noninvasive carcinoma	Fibroadenoma	Cyst
Invasive carcinoma (25)	20 (80.0%)	2 (8.0%)	3 (12.0%)	0 (0.0%)
Noninvasive carcinoma (15)	1 (6.7%)	11 (73.3%)	3 (20.0%)	0 (0.0%)
Fibroadenoma (26)	2 (7.7%)	1 (3.8%)	22 (84.6%)	1 (3.8%)
Cyst (17)	0 (0.0%)	0 (0.0%)	3 (17.6%)	14 (82.4%)

5. Discussion

Figure 19-23 show the distributions of the nine objective features obtained from all breast masses in our database. Here, these objective features were normalized by use of all cases in the database. Figure 19 shows the relationship between indistinctness in margin and depth-width ratio. The indistinctness in margin and depth-width ratio for malignant masses tended to be larger than those for benign masses. The degree of indistinctness in margin for invasive carcinoma and noninvasive carcinoma appeared to be larger than that for cysts and fibroadenoma. Figure 20 shows the relationship between shape irregularity and circularity. The degree of circularity for cysts and fibroadenoma tended to be larger than those for invasive carcinoma and noninvasive carcinoma. Figure 21 shows the relationship between intensity of echo-level in internal echoes and heterogeneousness in internal echoes. The intensity of echo-level in internal echoes and heterogeneousness in internal echoes for invasive carcinoma and noninvasive carcinoma tended to be larger than those for cysts and fibroadenoma. Figure 22 shows the relationship between lateral shadows and attenuation of echo-level in posterior echoes. The lateral shadow for cysts and fibroadenoma tended to be larger than those for benign masses. Figure 23 shows the relationship irregularity in margin and indistinctness in margin. The irregularity in margin for invasive carcinomas and noninvasive carcinomas tended to be larger than those for benign masses. These objective features for each histological classification appeared the tendency similar to the clinical characteristics. Therefore, we consider that the extraction methods of each objective features were appropriate to objectify clinician's subjective impression for image features.

Table II shows the result of test for univariate equality of group means. The Wilk's lambdas [19] for the degree of indistinctness in margin were smaller than that for the other objective features. The F-value [19] for the degree of indistinctness in margin was also larger than that for

any other features. This result would indicate that the degree of indistinctness in margin made a larger contribution to identifying four histological classifications of breast masses. On the other hand, the depth-width ratio of mass had the largest Wilk's lambda and the smallest F-value. The depth-width ratio made some contributions to the classification. However, the p value for the depth-width ratio of mass reached the level of statistical significance ($p < 0.05$). Thus, these nine objective features were statistically useful histological classifications of breast masses on ultrasonographic images. In the further study, we will examine our proposed method in clinical site.

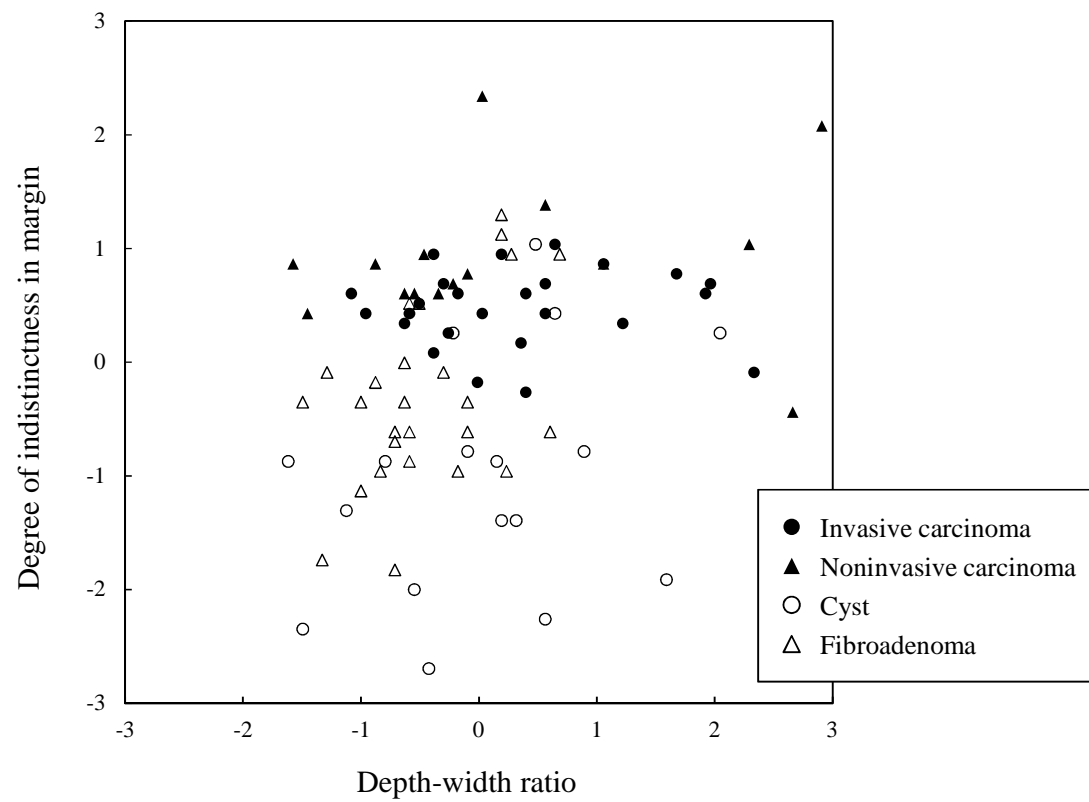


Figure 19 Relationship between depth-width ratio and degree of indistinctness in margin.

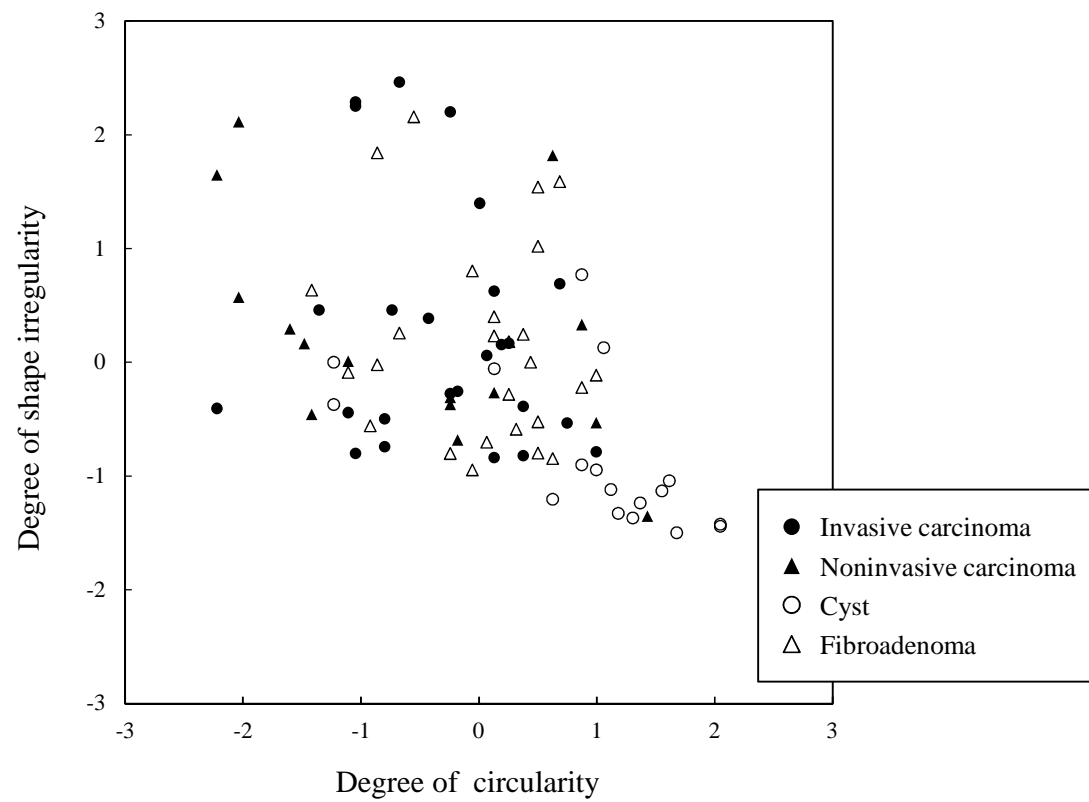


Figure 20 Relationship between degree of circularity and degree of shape irregularity.

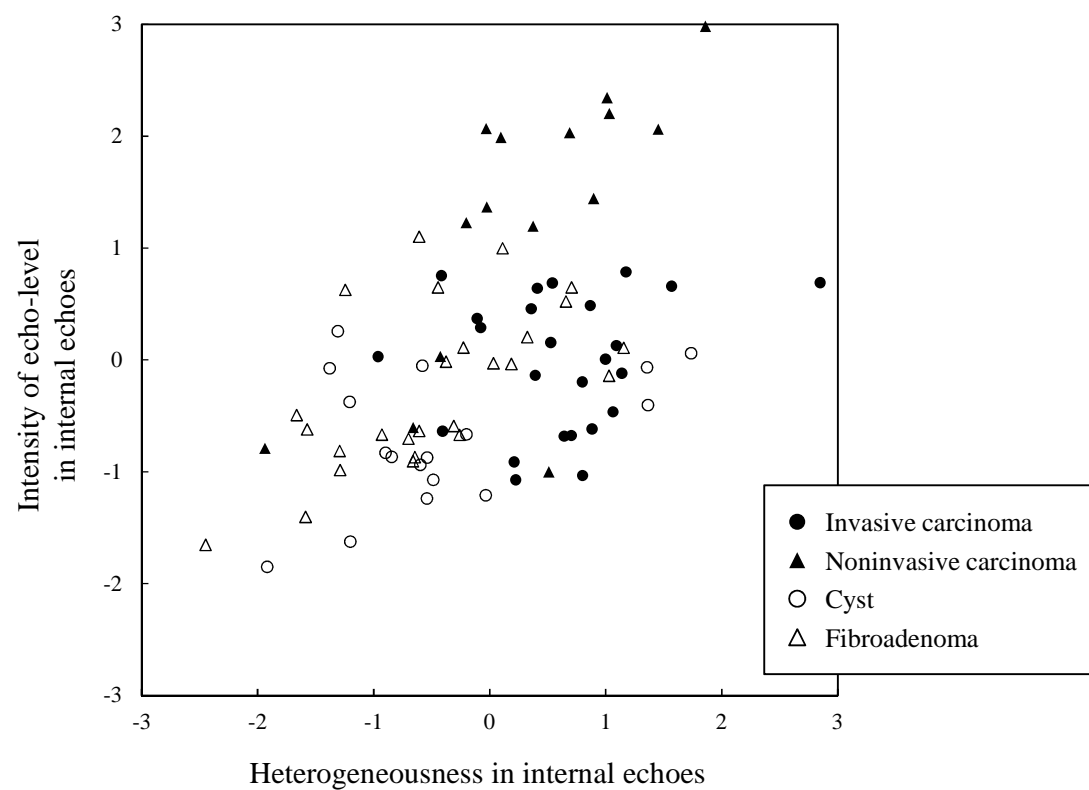


Figure 21 Relationship between heterogeneousness in internal echoes and intensity of echo-level in internal echoes.

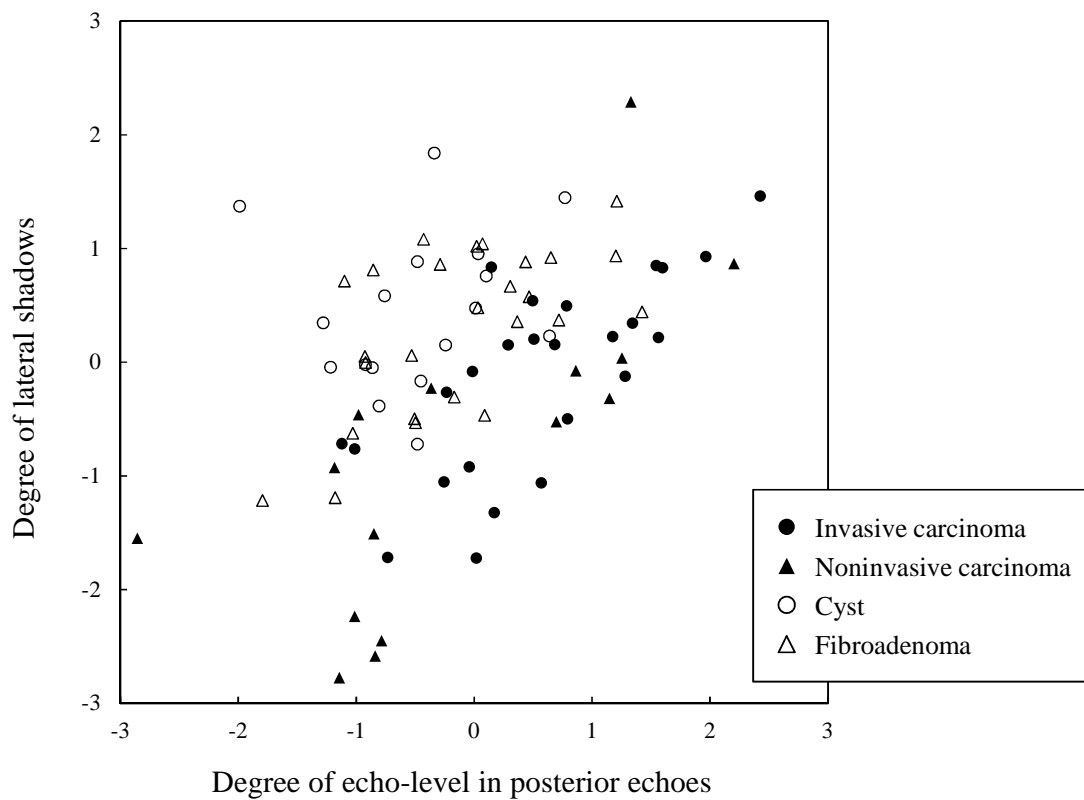


Figure 22 Relationship between degree of echo-level in posterior echoes and degree of lateral shadows.

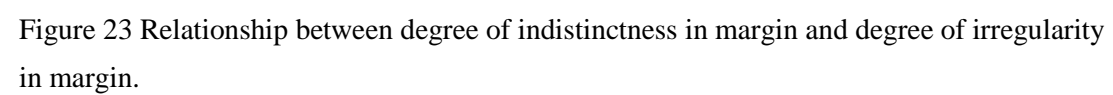


Table III Tests for univariate equality of group means.

	Wilk's lambda	<i>F</i> value	<i>p</i> value
The degree of circularity	0.727	9.913	$p < 0.05$
The degree of shape irregularity	0.817	5.896	$p < 0.05$
Depth-width ratio	0.892	3.183	$p < 0.05$
The degree of indistinctness in margin	0.529	23.450	$p < 0.05$
The degree of irregularity in margin	0.777	7.561	$p < 0.05$
The heterogeneousness in internal echoes	0.756	8.518	$p < 0.05$
The intensity of echo-level in internal echoes	0.602	17.422	$p < 0.05$
The degree of echo-level in posterior echoes	0.846	4.788	$p < 0.05$
The degree of lateral shadows	0.799	6.617	$p < 0.05$

6. Conclusion

In this study, we developed a computerized classification method for determining histological classifications of breast masses on ultrasonographic images. With our proposed method based on the leave-one-out testing method, the classification accuracies were 80.0% (20/25) for invasive carcinomas, 73.3% (11/15) for noninvasive carcinomas, 82.4% (14/17) for cysts, and 84.6% (22/26) for fibroadenomas, respectively. Our proposed method was shown to have high classification accuracies for histological classification, would be useful in the differential diagnosis of breast masses on ultrasonographic images for diagnosis aid.

Acknowledgement

I'm grateful to Prof. Shinji Tsuruoka at the graduate school of regional innovation studies, Mie University, Associate Prof. Haruhiko Takase, and Assistant Prof. Hiroharu Kawanaka at the graduate school of engineering, Mie University, for useful advice and to Assistant Prof. Ryohei Nakayama at Mie University School of Medicine for teaching and discussions. Many thanks are due to the members of Information Processing Laboratory in School of Engineering, Mie University.

References

- [1] American Cancer Society, "Cancer Facts and Figures 2010", (2010).
- [2] Center for Cancer Control and Information Services, National Cancer Center, Japan, "Cancer mortality", (2009).
- [3] D. R. Chen, R. F. Chang, and Y. L. Huang, "Computer-aided diagnosis applied to US of solid breast nodules by using neural networks," *Radiology*, vol.213, 407-412, (1999).
- [4] S. Joo, YS. Yang, WK. Moon, HC. Kim, "Computer-aided diagnosis of solid breast nodules: Use of an artificial neural network based on multiple sonographic features," *IEEE Trans Med Imaging*, 23(10): 1292-1300, (2004).
- [5] P. G. Nicholasas, D. Karen, L. G. Maryellen, S. A. Charlene, P. L. Lorenzo, "Performance of Breast Ultrasound Computer-aided Diagnosis : Dependence on image selection," *Academic Radiology*, 15(10): 1234–1245, (2008).
- [6] D. B. Kopans, *Breast Imaging*, 2nd ed. (Lippincott-Raven, New York), (1997).
- [7] G. Sakamoto and S.Haga, *Fundamental and Clinic of Ductal Carcinoma in Situ* (Sinoharashinsha, Tokyo), (2001).
- [8] M.Kass, A.Witkin, and D.Terzopoulos, "Snake: Active contour models," *Int.J.Compu.Vis.*, vol.1, 321-331 (1987).
- [9] C.Xu, and J.L Prince, "Gradient Vector Flow: A new External Force Snakes" , *Proc.IEEE Conf. on Comp. Vis. Pat. Recog. (CVPR)*, Los Alamitos: Comp.Soc.Press, pp.66-71, (1997).
- [10] C.Xu and J.L Prince, "Snakes, Shapes, and Gradient Vector Flow" *IEEE Trans. Image Processing*, vol.7, No.3, 359-369 (1998).
- [11] J.L. Su, H.Y. Lai, C.Y. Lo, H.Y Chang, and Y.C. Chang, "The Selection of Characteristic for Lesions Image in X-Ray Mammography and Breast Sonography for Computer-Aided

- Diagnosis System Development,” IFMBE proceedings, World congress on Medical Physics and Biomedical Engineering, Vol.14, pp.2487-2491, (2006).
- [12] R. C. Gonzales, R. E. Woods, Digital Image Processing, 2nd ed, MA: Addison-Wesley, 567-643 (1992).
- [13] The Japan Association of Breast and Thyroid Sonology, “Breast ultrasound diagnosis for Guideline,” Nankodo, 2004, (Japanese).
- [14] Phraseology and commission of diagnosis criterion of the japan society of ultrasonics in medicine, “Breast disease ultrasound diagnosis for guideline,” Japanese Journal of Medical Ultrasonics, vol.32, No.6, pp589-600, (2005), (Japanese).
- [15] R.O.Duda, P.E.Hart, and D.G.Stork, Pattern Classification, 2nd ed. (Wiley, New York, 2001).
- [16] M.Aoyama, Q. Li, S.Katsuragawa, H.MacMahon, K.Doi, “Automated computerized scheme for distinction between benign and malignant solitary pulmonary nodules on chest images,” Med Phys, 29, 701-708, (2002).
- [17] Ludmila I. Kuncheva, “Combining Pattern Classifiers: Methods and Algorithms”, Wiley-Interscience, (2004).
- [18] C.P.Langlotz, “Fundamental measures of diagnostic examination performance: Usefulness for clinical decision making and research,” Radiology, 228, 3-9 (2003).
- [19] R.A.Johnson and D.W.Wichern, *Applied Multivariate Statistical Analysis*. Englewood Cliffs, NJ: Prentice-Hall, (1992).

Research Accomplishment

国際会議（口頭・査読有）

- [1] Akiyoshi Hidukuri, Ryohei Nakayama, Toshihito Kawamura, Takanori Ogino, Shinji Tsuruoka, “Computerized Segmentation Method of Calcifications within Clustered Microcalcifications on Mammograms,” Proceedings of the First International Workshop on Regional Innovation Studies - Biomedical Engineering - (IWRIS2009), pp.47-50, Mie, Japan, (2009).
- [2] Takanori Ogino, Ryohei Nakayama, Toshihito Kawamura, Akiyoshi Hidukuri, Kan Takeda, “Computer-aided Detection Scheme for Sentinel Lymph Nodes,” Proceedings of the First International Workshop on Regional Innovation Studies - Biomedical Engineering - (IWRIS2009), pp.43-46, Mie, Japan, (2009).
- [3] Toshihito Kawamura, Ryohei Nakayama, Takanori Ogino, Akiyoshi Hidukuri, Hiroharu Kawanak, Shinji Tsuruoka, “Computerized Extraction Method of Hepatic Vessels in Contrasted Abdominal X-ray CT Images,” Proceedings of the First International Workshop on Regional Innovation Studies - Biomedical Engineering - (IWRIS2009), pp.51-54, Mie, Japan, (2009).
- [4] Akiyoshi Hizukuri, Ryohei Nakayama, Nobuo Nakako, Naoki Nagasawa, Shigeki Kobayashi, Kan Takeda, Shinji Tsuruoka, “Introduction of Computerized Detection Method to Breast Cancer Screening in Mie Prefecture,” Proceedings of the Second International Workshop on Regional Innovation Studies (IWRIS2010), pp.17-20, Mie, Japan, (2010).
- [5] Akiyoshi Hizukuri, Ryohei Nakayama, Nobuo Nakako, Takanori Ogino, Hiroharu Kawanaka, Haruhiko Takase, Shinji Tsuruoka, “Computerized identification method for current dental intraoral radiographs based on the arranged previous dental intraoral

radiographs,” Proceedings of the Second International Workshop on Regional Innovation Studies (IWRIS2010), pp.21-24, Mie, Japan, (2010).

- [6] Ryohei Nakayama, Yumi Kashikura, Akiyoshi Hizukuri, Shigeki Kobayashi, Kan Takeda, Tomoko Ogawa, “Computer-aided Diagnosis Scheme for Determining Histological Classifications of Breast Masses on Ultrasonographic Image” , Radiological Society of North America 2010 95st Scientific Assembly and Annual Meeting (RSNA2010), Chicago, (2010).

(ポスター・査読有)

- [7] Akiyoshi Hizukuri, Ryohei Nakayama, Toshihito Kawamura, Kan Takeda, Shinji Tsuruoka, “Computerized segmentation method of calcifications within clustered microcalcifications on mammograms using multiresolution analysis,”Computer Assisted Radiology and Surgery , Geneva, Switzerland, (2010).
- [8] Akiyoshi Hizukuri, Ryohei Nakayama, Yumi Kashikura, Nobuo Nakako, Tomoko Ogawa, Shinji Tsuruoka, “Computer-aided diagnosis scheme based on histological classifications of breast masses on ultrasonographic images,” Assisted Radiology and Surgery, Berlin, Germany, 2011.(Accepted).
- [9] Ryohei Nakayama, Akiyoshi Hizukuri, Toshihito Kawamura, Takanori Ogino, Naoki Nagasawa, Kan Takeda, “Computer-Aided diagnosis (CAD) scheme for detection of sentinel lymph nodes on lymphoscintigrams based on symmetry of mapped injection site.” Computer Assisted Radiology and Surgery, Geneva, Switzerland, (2010).

国内会議による発表

[口頭発表・査読有]

- [1] 川村敏仁, 中山良平, 荻野隆法, 檜作彰良, 竹田寛, 川中普晴, 高田考広, 山本皓二, 鶴岡信治, “乳房 X 線画像 (MLO 画像) を対象とした乳頭領域検出法の開発”, 第 28 回医療情報学連合大会, pp1179-1182, (2008).
- [2] 荻野隆法, 中山良平, 川村敏仁, 檜作彰良, 高田考広, 竹田寛, 山本皓二, “リンパシンチグラムにおけるセンチネルリンパ節部位のコンピュータ同定支援システムの開発”, 第 28 回医療情報学連合大会, pp1191-1193, (2008).
- [3] 中山良平, 檜作彰良, 中子敦雄, 永澤直樹, 小林茂樹, 竹田寛, “遠隔画像診断ネットワークへの CAD システム導入の可能性”, 日本乳癌検診学会誌, 19(3): 328, (2010).
- [4] 中子敦雄, 永澤直樹, 小林茂樹, 中山良平, 檜作彰良, 高田孝広, 竹田寛, “超高速回線を用いたマンモグラフィ遠隔画像診断システムの実用化”, 日本乳癌検診学会誌, 19(3): 328, (2010).

[口頭発表・査読なし]

- [5] 檜作彰良, 中山良平, 川村敏仁, 荻野隆法, 川中普晴, 高瀬治彦, 鶴岡信治, “対称性に基づいた差分処理によるセンチネルリンパ節の同定法,” 平成 21 年電気関係学会東海支部連合大会, O-203,名古屋, (2009).
- [6] 檜作彰良, 中山良平, 川村敏仁, 荻野隆法, 川中普晴, 鶴岡信治, “形状を維持した個々の石灰化陰影の抽出法,” 平成 20 年三重地区計測制御研究講演会, B21-B24, 三重, (2008).
- [7] 川村敏仁, 中山良平, 荻野隆法, 檜作彰良, 川中普晴, 鶴岡信治, “差分技術を用いたリンパシンチグラムにおけるセンチネルリンパ節のコンピュータ同定システ

ム,” 平成 20 年三重地区計測制御研究講演会, B11-B14, 三重, (2008 年).

- [8] 荻野隆法, 中山良平, 川村敏仁, 檜作彰良, 高田孝広, 山本皓二, 竹田寛, “リンパシンチグラムにおける注射部位の対称性に基づくセンチネルリンパ節の同定法,” 平成 20 年三重地区計測制御研究講演会, B11-B14, 三重, (2008 年).
- [9] 川村敏仁, 中山良平, 荻野隆法, 檜作彰良, 川中普晴, 鶴岡信治, “腹部 3 次元 CT 画像における肝臓領域内血管の抽出法,” 日本生体医工学会東海支部大会, p24, 愛知, (2009 年).

研究会

- [1] 檜作彰良: 三重県のマンモグラフィ検診のためのコンピュータ検出支援システム, みえメディカル研究会電子システム研究会 (三重大学), 10 月 28 日 一般講演, (2010).